Nov 11th, 12:00 AM

Earthquake Response of Locally Buckled Frames

George E. Blandford

Gordon C. Glass

Eighth International Specialty Conference on Cold-Formed Steel Structures
St. Louis, Missouri, U.S.A., November 11-12, 1986

EARTHQUAKE RESPONSE OF LOCALLY BUCKLED FRAMES

By

George E. Blandford[1] and Gordon C. Glass[2]

SUMMARY

The earthquake response of a thin-walled steel plane frame in the post-local-buckling range including first-order geometric nonlinearity is presented. Post-local-buckling behavior is included using the effective width concept utilizing both axial and bending stresses. An exact elastic stiffness, finite element geometric stiffness, consistent mass and Rayleigh damping matrix formulation is used to discretize the dynamic equilibrium equations. The nonlinear dynamic equations are solved using a modified Newton-Raphson iteration strategy coupled with the Newmark time integration scheme. Earthquake simulation results are presented for a two story, two bay frame composed of thin-walled members subjected to 1/2 the N-S component of the 1940 El Centro ground acceleration record. The results include linear elastic, local buckling and/or first-order geometric nonlinear simulations.

INTRODUCTION

Numerous papers have been written on the earthquake analysis of framework structural systems. However, the inclusion of local buckling on the response of structural systems is lacking. Therefore, the influence of reduced stiffness caused by local buckling on the response of frame structures requires investigation.

The purpose of this paper is to present the earthquake analysis results obtained using the program DYNFAP (DYnamic Nonlinear Frame Analysis Program). DYNFAP is a microcomputer program for the nonlinear static and dynamic analysis of steel structures composed of thin-walled members. Nonlinearities include post-local-buckling behavior as well as beam-column and P-delta effects.

DYNFAP uses the effective width concept (12) to represent the post-local-buckling strength in the compression plate elements of the frame members. Most research utilizing the effective width concept has been limited to static analysis, e.g. Refs. (6, 11 and 12). However, re-

---

[1] Associate Professor, Department of Civil Engineering, University of Kentucky, Lexington, KY 40506-0046

[2] Structural Engineer, Watkins and Associates, Inc., Lexington, KY

search conducted by Culver, et al. (4, 5, 9 and 13) on beams and columns has shown that the effective width concept is also valid for dynamic analysis. The inclusion of post-local-buckling behavior results in varying axial and flexual rigidities along the frame member lengths.

Previous research by the first author on the dynamic response of plane frames in the post-local-buckling range (2 and 3) has been based on using a Wilson-θ temporal discretization, an exact representation of the element elastic stiffness matrix and fixed-end forces in the post-local-buckling range, and a consistent finite element formulation for the first-order geometric nonlinear stiffness and mass matrices. An incremental (2) or load correction (3) scheme has been used to solve the nonlinear static/dynamic equations. DYNFAP uses Newmark's (7) time integration scheme to temporally discretize the dynamic equilibrium equations and modified Newton-Raphson iteration is used for the solution of the nonlinear equations. Additional DYNFAP features include: (i) initial static analysis to establish the structure forces and displacements for time invariant applied loading, (ii) lumped nodal mass representation of the inertia resistance for the time invariant loads, (iii) a Rayleigh damping matrix representation of the viscous damping forces and (iv) earthquake ground acceleration loading of the structure. These features of DYNFAP are discussed in the following sections of the paper along with results obtained from subjecting a plane frame composed of thin-walled members to 1/2 of the 1940 El Centro earthquake. Simulation results include linear elastic, local buckling and/or first-order geometric nonlinear analyses.

POST-LOCAL-BUCKLING STRENGTH

The static and dynamic analysis of frames composed of sufficiently thin-walled members must include the post-local-buckling response of the compression plate elements comprising the member and the interaction of the buckled elements with the other elements of the section. Winter (12) devised an experimental modification of von Karman's (10) effective width expression to incorporate the post-local-buckling strength which has been used extensively and successively for uniformly compressed thin-walled elements. A more recent effective width equation (6, 11) to calculate the post-local-buckling strength is

$$\frac{b}{t} = 0.95\sqrt{\frac{KE}{\sigma_{max}}}\left(1 - 0.95\xi\,\frac{t}{w}\sqrt{\frac{KE}{\sigma_{max}}}\right) \qquad (1)$$

for

$$\frac{w}{t} \geq 0.64\sqrt{\frac{KE}{\sigma_{max}}} \qquad (2)$$

in which b is the effective width of the compression plate element, w is the flat width, σ_{max} is the maximum edge stress, K is a coefficient determined by boundary conditions and aspect ratio for the compression plate element, E is the elastic modulus and ξ is a modification factor

based on experimental evidence and engineering judgement to incorporate local imperfections into the equation. For values of w/t smaller than $0.64\ KE/\sigma_{max}$, b = w.

Equation 1 has been shown through experimental verification to be applicable to both stiffened and unstiffened plate elements if K is appropriately adjusted. For uniformly compressed sections, K varies from 4.00 to 6.97 for stiffened plate elements and from 0.425 to 1.28 for unstiffened plate elements. For design considerations, ξ may be considered equal to 0.22 and K may be taken to be 0.50 and 4.0 for unstiffened and stiffened plate elements, respectively.

Post-local-buckling strength for frames is best understood by considering the rigid plane frame of Fig. 1(a). The compression plate elements of the frame members will buckle locally and the neutral axis will shift away from the compression plate element as shown in Fig. 1(c). This occurs provided the compression element(s) stress is larger than the local buckling stress σ_{cr}. (Neutral axis shift varies along the member due to nonuniform moment distribution as shown in Fig. 1(b).)

The local buckling stress is derived from Eq. 2 by replacing σ_{max} with σ_{cr} and solving for σ_{cr}, i.e.,

$$\sigma_{cr} = 0.41 \frac{KE}{(w/t)^2} \tag{3}$$

For regions along the member length with compression elements stressed at levels larger than σ_{cr}, the reduced effective flexural rigidity EI_{eff} and axial rigidity EA_{eff} varies along the member length depending upon the stress magnitude. Thus, in the post-local-buckling range, the frame is composed of nonprismatic members as shown schematically in Fig. 1(d). Consequently, post-local-buckling behavior introduces a nonlinear elastic material property (provided yielding does not occur) into the frame problem.

DYNAMIC EQUILIBRIUM

The dynamic equilibrium equations can be obtained from d'Alembert's principle to give

$$^{t}\{F_I\} + {}^{t}\{F_D\} + {}^{t}\{F_E\} = {}^{t}\{P\} \tag{4}$$

where $^{t}\{F_I\}$, $^{t}\{F_D\}$, $^{t}\{F_E\}$ and $^{t}\{P\}$ are the inertial, damping, elastic and external load vectors, respectively at time t. Evaluating Eq. 4 at time $t + \Delta t$, where Δt is the time increment, and writing the nonlinear portion of the resulting equation in incremental form leads to

$$^{t+\Delta t}\{F_I\} + {}^{t+\Delta t}\{F_D\} + \{dF_E\} = {}^{t+\Delta t}\{P\} - {}^{t}\{F_E\} \tag{5}$$

where d is used to signify the increment between time t and time t+Δt.

The matrix form of Eq. 5 which includes first-order geometric nonlinearity (beam-column and P-delta effects), a Rayleigh damping approximation and horizontal ground accelerations is

$$[M]\ {}^{t+\Delta t}\{\ddot{v}\} + [C]\ {}^{t+\Delta t}\{\dot{v}\} + ({}^{t}[K_E] + {}^{t}[K_G])\ \{dv\} = {}^{t+\Delta t}\{P\} - [M]\ \{r\}\ {}^{t+\Delta t}\ddot{v}_g - {}^{t}\{F_E\} \quad (6)$$

In Eq. 6 [M] is the structure mass matrix (assumed linear), [C] is the Rayleigh damping matrix (assumed linear), i.e.

$$[C] = a_0\ [M] + a_1\ {}^{0}[K_E] \quad (7)$$

where a_0 and a_1 are the coefficients of proportionality for the mass and elastic stiffness matrices respectively, $[K_E]$ is the structure tangent elastic stiffness matrix (nonlinear in the post-local-buckling range), $[K_G]$ is the structure tangent geometric stiffness matrix, $\{\ddot{v}\}$ is the acceleration vector, $\{\dot{v}\}$ is the velocity vector, $\{dv\}$ is the incremental displacement vector, $\{r\}$ contains zeros and ones arranged such that the earthquake ground acceleration, $\ddot{v}_g$, excites the horizontal displacement degrees of freedom, the pre-superscript signifies time level at which the matrix variable is evaluated and the superposed dots signify the order of time differentiation. The matrices and vectors of Eq. 6 are obtained using standard coordinate transformation techniques on the element level equations and direct stiffness assembly.

TIME INTEGRATION SCHEME

Equation 6 shows that the dynamic equilbrium equations require a temporal discretization in addition to the spacial discretization presented in the previous section. This investigation utilizes Newmark's (7) direct time integration scheme. Newmark's discretization method employs the following velocity and displacement variations

$${}^{t+\Delta t}\{\dot{v}\} = {}^{t}\{\dot{v}\} + \Delta t[(1 - \delta)\ {}^{t}\{\ddot{v}\} + \delta\ {}^{t+\Delta t}\{\ddot{v}\}] \quad (8)$$

$${}^{t+\Delta t}\{v\} = {}^{t}\{v\} + \Delta t\ {}^{t}\{\dot{v}\} + \Delta t^2\ [(1/2 - \alpha)\ {}^{t}\{\ddot{v}\} + \alpha\ {}^{t+\Delta t}\{\ddot{v}\}] \quad (9)$$

where α and δ are parameters chosen to obtain integration accuracy and stability. Newmark proposed the unconditionally stable constant-average acceleration scheme (also known as the trapezoidal rule) in which $\delta = 1/2$ and $\alpha = 1/4$.

Due to the stress dependent stiffness matrices in Eq. 6 the application of Newmark's assumptions (Eqs. 8 and 9) cannot be directly utilized. Instead an iteration technique should be used to ensure equilibrium within each time increment. The nonlinear solution strategy is discussed in the following section.

NONLINEAR SOLUTION STRATEGY

The solution of the nonlinear dynamic equilbrium equations requires a system level iteration scheme and an iteration technique to calculate the quadrature point effective constitutive properties for the beam elements in the post-local-buckling range (15 point composite Simpson rule is used to evaluate the element elastic stiffness matrices and fixed-end force vectors in the post-local-buckling range (3)). System level iteration is based on modified Newton-Raphson iteration whereas the quadrature point constitutive properties are calculated using direct iteration.

A modified Newton-Raphson iteration strategy for Eq. 6 is (1)

$$[M]\ {}^{t+\Delta t}\{\ddot{v}\}^{(k)} + [C]\ {}^{t+\Delta t}\{\dot{v}\}^{(k)} + ({}^{t}[K_E] + {}^{t}[K_G])\ \{dv\}^{(k)}$$
$$= {}^{t+\Delta t}\{P\}^{(k-1)} - [M]\ \{r\}\ {}^{t+\Delta t}\ddot{v}_g - {}^{t+\Delta t}\{F_E\}^{(k-1)} \qquad (10)$$

where k = 1, 2, ... is the iteration number and

$${}^{t+\Delta t}\{F_E\}^{(0)} \equiv {}^{t}\{F_E\}$$
$${}^{t+\Delta t}\{v\}^{(0)} \equiv {}^{t}\{v\}$$
$${}^{t+\Delta t}\{v\}^{(k)} = {}^{t+\Delta t}\{v\}^{(k-1)} + \{dv\}^{(k)} \qquad (11)$$

The iteration number on the load vector signifies that the fixed-end force vector is dependent on the stiffness distribution in the post-local-buckling range. Newmark's temporal discretization (Eqs. 8 and 9) for the modified Newton-Raphson iteration scheme is (1)

$${}^{t+\Delta t}\{\dot{v}\}^{(k)} = {}^{t}\{\dot{v}\} + \Delta t\ [(1-\delta)\ {}^{t}\{\ddot{v}\} + \delta\ {}^{t+\Delta t}\{\ddot{v}\}^{(k)}] \qquad (12)$$

$${}^{t+\Delta t}\{v\}^{(k)} = {}^{t}\{\dot{v}\} + \Delta t\ {}^{t}\{\ddot{v}\} + \Delta t^2\ [(\tfrac{1}{2} - \alpha)\ {}^{t}\{\ddot{v}\} + \alpha\ {}^{t+\Delta t}\{\ddot{v}\}^{(k)}] \qquad (13)$$

Solving Eq. 13 for the accelearation gives

$${}^{t+\Delta t}\{\ddot{v}\}^{(k)} = \frac{1}{\alpha \Delta t^2}\ ({}^{t+\Delta t}\{v\}^{(k)} - {}^{t}\{v\}) - \frac{1}{\alpha \Delta t}\ {}^{t}\{\dot{v}\}$$
$$+ (1 - \frac{1}{2\alpha})\ {}^{t}\{\ddot{v}\} \qquad (14)$$

which is used to update the acceleration vector. Similarly, the updated velocity vector can be obtained by substituting Eq. 14 into Eq. 12 to give

$${}^{t}\{\dot{v}\}^{(k)} = \frac{\delta}{\alpha \Delta t}\ ({}^{t+\Delta t}\{v\}^{(k)} - {}^{t}\{v\})$$

$$+ \left(1 - \frac{\delta}{\alpha}\right) {}^{t}\{\dot{v}\} + \Delta t \left(1 - \frac{\delta}{2\alpha}\right) {}^{t}\{\ddot{v}\} \tag{15}$$

Substituting Eq. 11 into Eqs. 14 and 15 and then substituting the resulting equations into Eq. 10 leads to

$${}^{t}[\bar{K}] \{dv\}^{(k)} = {}^{t+\Delta t}\{\bar{P}\}^{(k-1)} - {}^{t+\Delta t}\{F_E\}^{(k-1)} \tag{16}$$

where

$${}^{t}[\bar{K}] = \frac{1}{\alpha \Delta t^2}[M] + \frac{\delta}{\alpha \Delta t}[C] + {}^{t}[K_E] + {}^{t}[K_G]$$

is the effective stiffness matrix,

$$\begin{aligned} {}^{t+\Delta t}\{\bar{P}\}^{(k-1)} &= {}^{t+\Delta t}\{P\}^{(k-1)} - [M]\{r\} {}^{t+\Delta t}\ddot{v}_g \\ &+ [M]\left\{ \frac{1}{\alpha \Delta t^2} \left({}^{t}\{v\} - {}^{t+\Delta t}\{v\}^{(k-1)}\right) \right. \\ &\left. + \frac{1}{\alpha \Delta t} {}^{t}\{\dot{v}\} + \left(\frac{1}{2\alpha} - 1\right) {}^{t}\{\ddot{v}\} \right\} \\ &+ [C]\left\{ \frac{\delta}{\alpha \Delta t} \left({}^{t}\{v\} - {}^{t+\Delta t}\{v\}^{(k-1)}\right) \right. \\ &\left. \left(\frac{\delta}{\alpha} - 1\right) {}^{t}\{\dot{v}\} + \Delta t \left(\frac{1}{2\alpha} - 1\right) {}^{t}\{\ddot{v}\} \right\} \end{aligned}$$

is the effective load vector and

$$\begin{aligned} {}^{t+\Delta t}\{F_E\}^{(k)} &= {}^{t+\Delta t}\{F_E\}^{(k-1)} + \left({}^{t+\Delta t}[K_E]^{(k-1)} \right. \\ &\left. + {}^{t+\Delta t}[K_G]^{(k-1)}\right) \{dv\}^{(k)} \end{aligned}$$

is the balanced (equilibrated) elastic load vector for iteration k. The balanced elastic load is actually calculated at the element level, transformed into the global coordinate system and then assembled.

Equation 16 is the modified Newton-Raphson system of equations which are iteratively evaluated to satisfy equilbrium for each time increment. Equation 16 can also be used to solve static problems simply by taking the mass and damping properties to equal zero. For a static analysis Δt is used to determine the stress (force) increment, but is otherwise a dummy variable.

Due to the number of simultaneous equations which must be solved in Eq. 16, the symmetric Gauss - Crout skyline (profile) assembly and solution algorithms of Taylor (8) are used. Taylor's skyline scheme minimizes matrix storage as well as the operation count associated with matrix factorization and back substitution.

Termination of the iterations in Eq. 16 is based on both the out-of-balance load and incremental internal energy criteria of Bathe and Cimento (1). The out-of-balance load criterion is

$$\frac{\| {}^{t+\Delta t}\{P\}^{(k-1)} - {}^{t+\Delta t}\{\tilde{F}\}^{(k-1)} \|_2^2}{\| {}^{t+\Delta t}\{P\}^{(0)} - {}^{t}\{F_E\} - {}^{t}\{F_D\} - {}^{t}\{F_I\} \|_2^2} < \epsilon_F$$

and the incremental internal energy criterion is

$$\frac{\lfloor dv \rfloor^{(k)} ({}^{t+\Delta t}\{P\}^{(k-1)} - {}^{t+\Delta t}\{\tilde{F}\}^{(k-1)})}{\lfloor dv \rfloor^{(1)} ({}^{t+\Delta t}\{P\}^{(0)} - {}^{t}\{F_E\} - {}^{t}\{F_D\} - {}^{t}\{F_I\})} < \epsilon_E$$

where ϵ_F is the force error tolerance ($1 \times 10^{-8} \leq \epsilon_F \leq 1 \times 10^{-4}$), ϵ_E is the energy error tolerance ($1 \times 10^{-8} \leq \epsilon_E \leq 1 \times 10^{-4}$), $\| \|_2^2$ signifies the square of the Eucledian two-norm and

$${}^{t+\Delta t}\{\tilde{F}\}^{(k-1)} \equiv {}^{t+\Delta t}\{F_E\}^{(k-1)} + {}^{t+\Delta t}\{F_D\}^{(k-1)} + {}^{t+\Delta t}\{F_I\}^{(k-1)}$$

$${}^{t+\Delta t}\{F_D\}^{(k)} = [C]\ {}^{t+\Delta t}\{\dot{v}\}^{(k)}$$

$${}^{t+\Delta t}\{F_I\}^{(k)} = [M]\ {}^{t+\Delta t}\{\ddot{v}\}^{(k)}$$

The nonlinear frame problems investigated in this paper required between 2 - 5 iterations per time step to satisfy the convergence criteria.

NUMERICAL RESULTS

Figure 2(a) shows the geometry, ℓ_b = 100 in (254 cm) and ℓ_c = 60 in (152.4 cm), and time invariant loading, q = 2.4 lbs/in (4.2 N/cm), for the frame considered in this paper. In addition to the uniform loads shown in Fig. 2(a), the frame is subjected to one-half of the horizontal N-S component of the 1940 El Centro earthquake ground acceleration record (earthquake duration of 53.76 sec in increments of Δt = 0.02 sec). Linear elastic (LE), first-order geometric nonlinear (GN), local buckling (LB) and combined local buckling and geometric nonlinear (LB+GN) simulations totally 60 seconds are considered. Each earthquake analysis uses Newmark's constant-average acceleration scheme (α = 1/4 and δ = 1/2) and is preceeded by a static analysis to generate the force and displacement results for the time invariant uniform loads. These uniform member loads are maintained during the earthquake excitation. Convergence tolerances for the nonlinear simulations have been set to $\epsilon_E = \epsilon_F = 1 \times 10^{-6}$.

Unbuckled member section properties for the frame are

$$A_0 = 0.26132 \text{ in}^2 \quad (1.6859 \text{ cm}^2)$$
$$I_0 = 0.10610 \text{ in}^4 \quad (4.4162 \text{ cm}^4)$$

where the member cross section is shown in Fig. 2(c). A uniform mass/length for the steel cross section of Fig. 2(b) is m = 0.002305 slugs/in (0.08551 kg/cm) which is used to construct the element consistent mass matrices. Lumped nodal masses have been used to account for the inertia resistance provided by the uniform load. Only the rectilinear degrees of freedom have been assigned lumped masses, no rotational lumped mass has been assigned for the load. Rayleigh damping coefficients for the frame of Fig. 2 are

$$a_0 = 0.211$$
$$a_1 = 0.00134$$

which have been calculated assuming two percent critical damping in the first two elastic structural response modes.

Table 1 gives the magnitude and time of occurence for the maximum and minimum values (maximum is defined as the largest positive value; mininum is defined as the largest negative value) of story sidesway displacements defined in Fig. 2(b) for each analysis. It is observed from Table 1 that the times of occurence remain fairly constant. The extreme values show that the GN behavior exhibits the largest sidesway displacement increase compared with the linear elastic response. With the exception of the minimum value of the second story displacement (Δ^2_{min}) for the LB+GN analysis, the values for both LB and LB+GN fall within the range of the GN analysis.

Figures 3(a)-(d) show the time variation of the top story sidesway displacement (Δ^2) response for the different analyses. Comparing Figs. 3(b), (c) and (d) with Fig. 3(a) shows that the nonlinear analyses generally match the linear elastic response during the first five seconds of the earthquake excitation except that the nonlinear simulations exhibit larger maximum and minimum peak values during this time period. From $t \approx 5$ to 11 sec the nonlinear results slightly shift out of phase with the LE results and exhibit lower amplitudes with the LB+GN simulation resulting in the lowest sidesway displacements. The nonlinear analyses exhibit a secondary surge for $t \approx 12$ to 18 sec compared with the low response exhibited by the LE analysis. This behavior in the nonlinear simulations for 5 sec $\leq t \leq$ 18 sec is probably due to the change in stiffness of the nonlinear models. A stiffness reduction decreases the circular frequencies which results in period extention of the vibration modes thus altering the degree of excitation experienced in each structural mode. Achieving peak responses during the first five seconds of the simulation results in a maximum reduced stiffness for 5 sec $\leq t \leq$ 11 sec resulting in peak inertia and damping resistance which causes a time delay in the structural response. For 11 sec $< t <$ 18 sec the stiffness increases relatively thus decreasing the importance of the inertia and damping resistance.

A comparison of the nonlinear analysis results with the LE analysis

results of Fig. 3(a) shows that the GN results (Fig. 3(b)) exhibit the largest difference for t < 30 sec whereas the LB+GN results (Fig. 3(d)) exhibit the largest difference for t > 30 sec. For t > 30 sec the LB results of Fig. 3(c) are nearly identical with the LE results. Ground acceleration excitation is relatively low for t > 30 sec and consequently there is less post-local buckling force redistribution because the structure loading becomes essentially symmetric. However, since the uniform loads remain throughout the simulation the columns maintain their reduced stiffness resulting from first-order geometric nonlinearity. This reduced column stiffness caused by first-order geometric nonlinearity plus the reduced beam stiffness caused by local buckling combines to produce the increased sidesway displacement exhibited by the LB+GN analysis.

Figures 4(a)-(d) show the time response of the base shear (base shear $\equiv F^1(t) + F^2(t) + F^3(t)$ where the superscripts are the column locations shown in Fig. 2(b)) for each analysis. The base shears allow the combination of earthquake accelerations and structural mass to be quantified in terms of the force required to resist it. In this case the one-half 1940 El Centro earthquake combined with the given structural mass to produce base shears of about 500 pounds (2225 N) for all analyses with the maximum base shear being 515 lbs (2292 N) for the GN analysis case. The linear elastic analysis results (Fig. 4 (a)) show a direct response to the earthquake excitation while the nonlinear analyses exhibit longer sustained amplitudes for t < 30 sec. Base shear for the local buckling case (Fig. 4(c)) exibits larger amplitudes during the pre 30 second period but are similar to the linear elastic response in the post 30 second period. Base shear response for the combined local buckling and geometric nonlinear case (Fig. 4(d)) has a lower magnitude response than either the GN case (Fig. 4(b)) or the LB case for t < 30 sec while showing larger amplitudes than either the GN or LB responses for t > 30 sec. Comparing Figs. 3 and 4 show that the base shear response is similar to the sidesway displacement response.

CONCLUSIONS

Conclusions obtained from the present study can be summarized as:

1. Stress redistribution caused by beam-column and P-delta (first-order geometric nonlinearity) effects has been shown to be more significant than that caused by local buckling for the problems considered. Consequently, first-order geometric nonlinearity should be included in the analysis and design of thin-walled steel structures.

2. Inclusion of both local buckling and geometric nonlinearities resulted in the largest percentage stress redistribution for low amplitude ground acceleration excitation as compared with the linear elastic results.

APPENDIX I - REFERENCES

1. Bathe, K. J. and Cimento, A. P., "Some Practical Procedures for the Solution of Nonlinear Finite Element Equations," Comp. Meth. Appl. Mech. Engrg., Vol. 22, 1980, pp. 59-85.

2. Blandford, G. E., Wang, S. T. and Wang, N. T., "Dynamic Behavior of Locally Buckled Frames," Proc. Sixth Int. Spec. Conf. Cold-Formed Steel Structures, St. Louis, MO, Nov. 1982, pp. 349-368.

3. Blandford, G. E., Wang, S. T. and Wang, N. T., "Geometric Nonlinear Dynamic Analysis of Locally Buckled Frames", Proc. Seventh Int. Spec. Conf. Cold-Formed Steel Structures, St. Louis, MO, Nov. 1984, pp. 167-187.

4. Culver, C. G. and Tassel, R. A., "Shock Loading of Thin Compression Elements," Proc. First Spec. Conf. Cold-Formed Steel Structures, Univ. Missouri - Rolla, MO, Aug. 1971, pp. 65-72.

5. Culver, C. G., Zanoni, E. A. and Osgood, A. H., "Response pf Thin-Walled Beams to Impact Loading," Proc. First Spec. Conf. Cold-Formed Steel Structures, Univ. Missouri - Rolla, MO, Aug. 1971, pp. 82-90.

6. Johnson, A. L. and Winter, G., "Behavior of Stainless Steel Columns and Beams," J. Struct. Div., ASCE, Vol. 95, No. ST5, 1968, pp. 97-118.

7. Newmark, N. M., "A Method of Computation for Structural Dynamics," J. Engrg. Mech. Div., ASCE, Vol. 85, 1959, pp. 67-94.

8. Taylor, R. L., in O. C. Zienkiewicz, The Finite Element Method, Third Edition, McGraw-Hill, New York, 1977, Chapter 24.

9. Vaidya, N. R. and Culver, C. G., "Impact Loading of Thin-Walled Columns," Proc. First Spec. Conf. Cold-Formed Steel Structures, Univ. Missouri - Rolla, MO, Aug. 1971, pp. 91-98.

10. von Karman, T., Sechler, E. E. and Donnell, L. H., "The Strength of Thin Plates in Compression," Trans., ASME, Vol. 54, 1932.

11. Wang, S. T., Errera, S. J. and Winter, G., "Behavior of Cold-Rolled Stainless Steel Members," J. Struct. Div., ASCE, Vol. 101, No. ST11, 1975, pp. 2337-2357.

12. Winter, G., "Strength of Thin-Walled Compression Flanges," Trans. ASCE, Vol. 112, 1947, pp. 527-555.

13. Zanoi, E. A. and Culver, C. G., "Impact Loading of Thin-Walled Beams," Proc. First Spec. Conf. Cold-Formed Steel Structures, Univ. Missouri - Rolla, MO, Aug. 1971, pp. 73-81.

APPENDIX II - NOTATION

The following symbols are used in this paper:

a_0 - mass proportionality constant for Rayleigh damping matrix,
a_1 - stiffness proportionality constant for Rayleigh damping matrix,
b - effective width of compression plate element,
d - symbol used to signify increment,
$\bar{m}$ - mass per unit length,
q - magnitude of uniform load,
t - plate thickness, or time,
Δt - time increment,
w - flat width of compression plate element exclusive of fillets,
A - area,
E - elastic modulus,
I - moment of inertia,
K - buckling coefficient,
M - moment,
$\ddot{v}_g$ - ground acceleration,
α and δ - Newmark time integration parameters,
ϵ_E - energy error convergence tolerance used in the modified Newton-Raphson iteration scheme,
ϵ_F - force error convergence tolerance used in the modified Newton-Raphson iteration scheme,
ℓ_b - beam length,
ℓ_c - column length,
σ - stress,
σ_{cr} - critical local buckling stress,
σ_{max} - maximum edge stress,
ξ - effective width modification factor,
Δ - story sidesway displacement, and
$\| \|_2^2$ - square of the Eucledian two-norm.

Subscripts

eff - effective section property in the post-local-buckling range, and
0 - unbuckled section property.

Superscripts

k	-	modified Newton-Raphson iteration counter,
t	-	evaluated at time t, and
$t + \Delta t$	-	evaluated at time $t + \Delta t$.

Vectors

$\{F_D\}$	-	internal damping force vector,
$\{F_E\}$	-	internal elastic force vector,
$\{F_I\}$	-	internal inertia force vector,
$\{P\}$	-	external load vector,
$\{\bar{P}\}$	-	effective load vector,
$\{r\}$	-	vector of ones and zeros to ensure that the horizontal degrees of freedom are directly excited by the earthquake ground accelerations,
$\{v\}$	-	structure displacement vector,
$\{\dot{v}\}$	-	structure velocity vector, and
$\{\ddot{v}\}$	-	structure acceleration vector.

Matrices

$[C]$	-	structure Rayleigh damping matrix,
$[K_E]$	-	structure tangent elastic stiffness matrix,
$[K_G]$	-	structure tangent geometric stiffness matrix,
$[\bar{K}]$	-	effective stiffness matrix, and
$[M]$	-	structure mass matrix.

Table 1. Sidesway Displacement Results for the El Centro Earthquake Analyses (1 in = 2.54 cm)

ANALYSIS	DISPLACEMENT (inches)	TIME (seconds)
LE	$\Delta^1_{max} = 1.709$	4.7
	$\Delta^1_{min} = -1.619$	4.3
	$\Delta^2_{max} = 3.782$	4.7
	$\Delta^2_{min} = -3.337$	4.3
GN	$\Delta^1_{max} = 1.928$	4.8
	$\Delta^1_{min} = -1.767$	4.3
	$\Delta^2_{max} = 3.951$	4.8
	$\Delta^2_{min} = -3.607$	4.3
LB	$\Delta^1_{max} = 1.896$	4.8
	$\Delta^1_{min} = -1.786$	4.3
	$\Delta^2_{max} = 3.851$	4.8
	$\Delta^2_{min} = -3.476$	4.3
LB+GN	$\Delta^1_{max} = 1.854$	4.8
	$\Delta^1_{min} = -1.836$	4.4
	$\Delta^2_{max} = 3.736$	4.8
	$\Delta^2_{min} = -3.751$	4.4

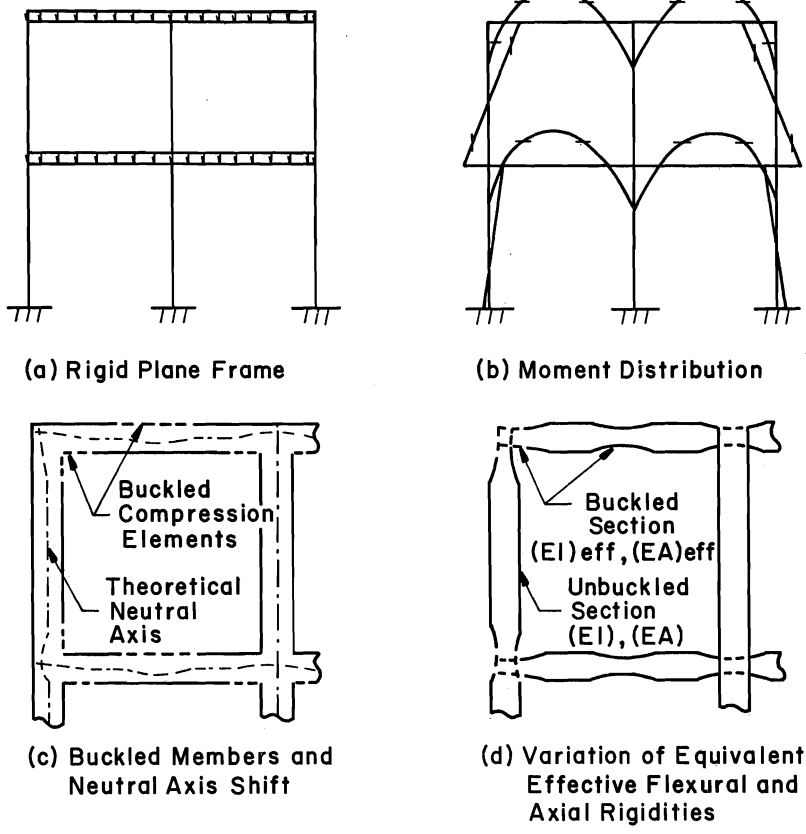

FIG. 1 - RIGID PLANE FRAME IN THE POST-LOCAL-BUCKLING RANGE

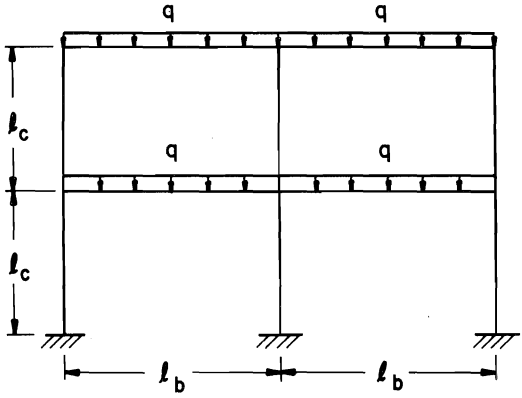

(a) Frame Geometry and Loading

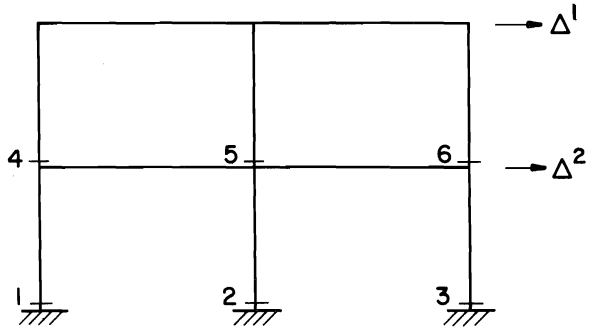

(b) Force and Displacement Locations

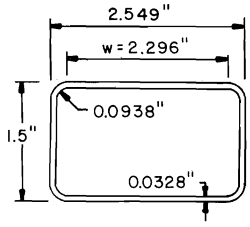

(c) Dimensions for Rectangular Tubular Section

FIG. 2 - TWO STORY, TWO BAY FRAME (1 in = 2.54 cm)

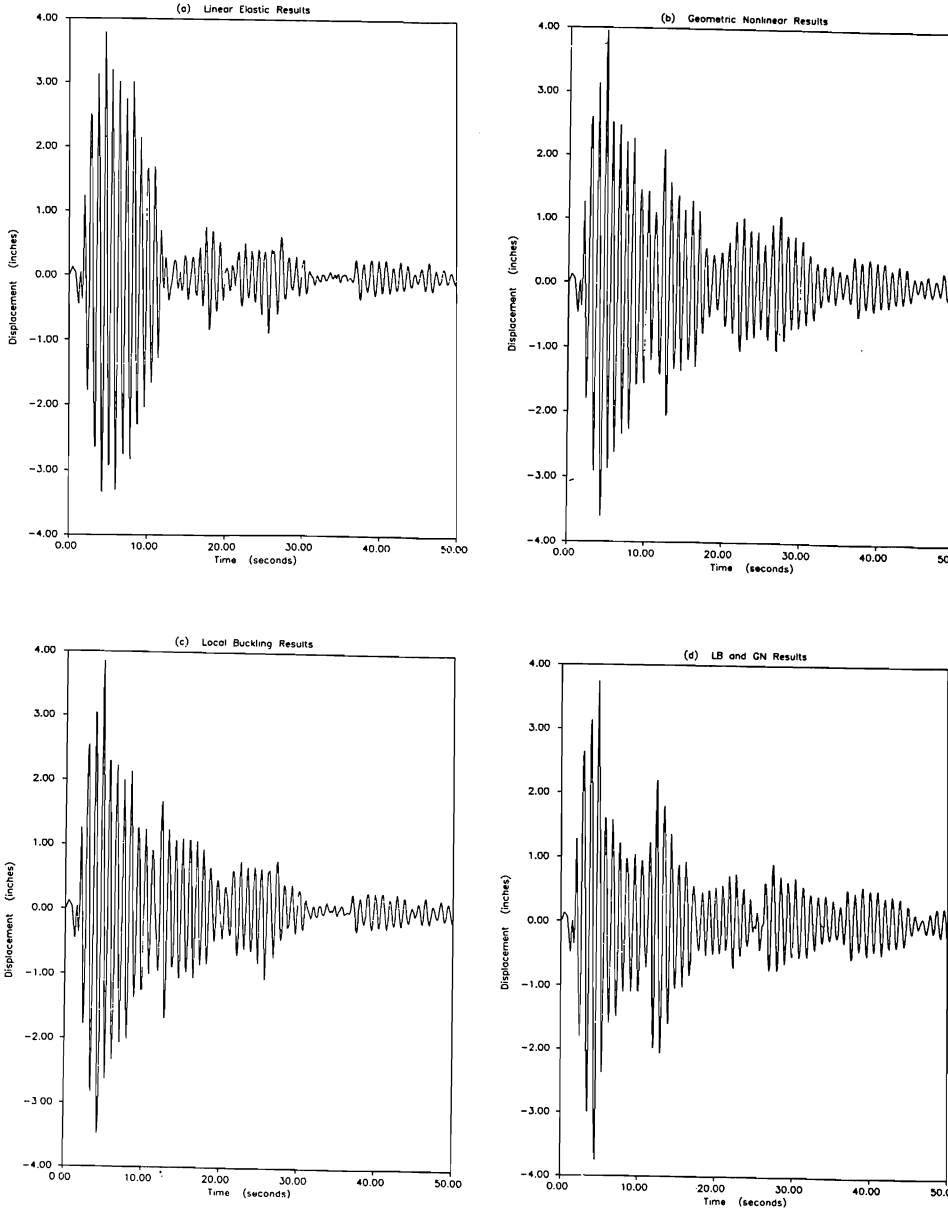

FIG. 3 - SIDESWAY DISPLACEMENT RESULTS (1 in = 2.54 cm)

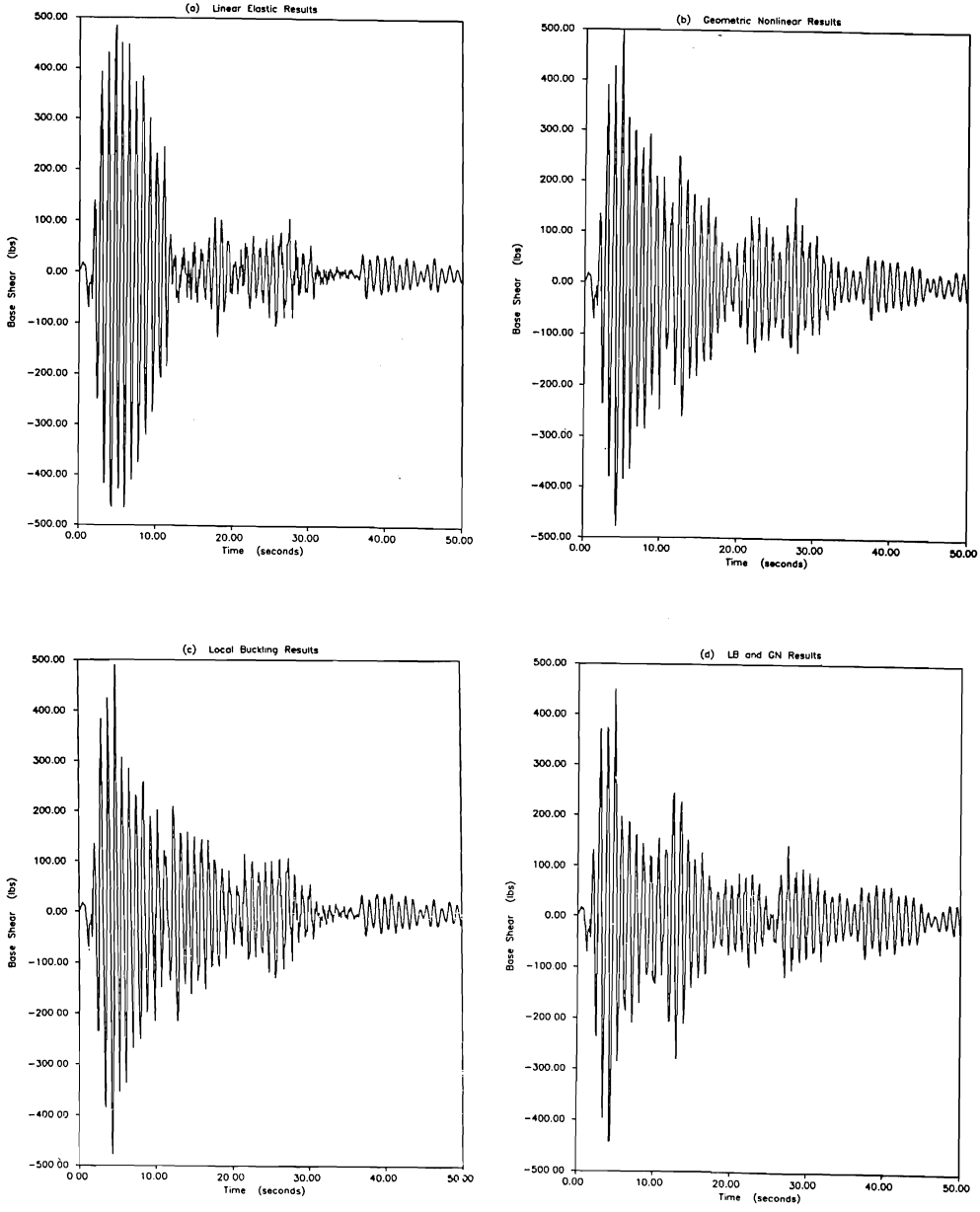

FIG. 4 - BASE SHEAR RESULTS (1 lb = 4.45 N)